International Communications in Heat and Mass Transfer 48 (2013) 46–52

Contents lists available at ScienceDirect

International Communications in Heat and Mass Transfer

journal homepage: www.elsevier.com/locate/ichmt

Heatline visualization for conjugate heat transfer of a couple stress fluid from a vertical slender hollow cylinder ☆

H.P. Rani *, G. Janardhana Reddy

Department of Mathematics, National Institute of Technology, Warangal 506004, AP, India

ARTICLE INFO

Available online 7 September 2013

Keywords:
Heat function
Conjugate heat transfer
Couple stress fluid
Natural convection
Vertical slender hollow cylinder

ABSTRACT

The flow visualization has been made using the heat function concept for the conjugate heat transfer effects on the transient free convective couple stress fluid flow over a vertical slender hollow circular cylinder with the inner surface kept at a constant temperature. The governing non-linear equations are solved numerically by using an unconditionally stable implicit method. Numerical results show that the deviations of flow variables of couple stress fluid from those of the Newtonian fluid turn out to be considerable. Boundary layer flow visualization indicates that the streamlines exist starting from the leading edge to the far downstream, while the heatlines terminate at a finite distance from the cylinder wall. It is noticed that the steady-state values of average skin-friction and heat transfer rate decrease as the conjugate-conduction parameter increases.

1. Introduction

Unsteady natural convective flow of a viscous incompressible fluid is an important problem relevant to many engineering applications. In the glass and polymer industries, hot filaments are considered as vertical cylinders and cooled as they pass through the surrounding environment. In most of these situations, the temperature distribution in the fluid is mutually coupled with the temperature distribution in the solid body over which the fluid flows. These types of problems are studied in-depth in the literature. It can be observed that in the previous investigations the wall conduction resistance in the case of convective heat transfer between a solid cylinder wall and a fluid flow is generally neglected i.e. the wall is assumed to be very thin [1,2]. But in many practical problems the information on the interfacial temperature is essential because the heat transfer characteristics are mainly determined by the temperature differences between the bulk flow and the interface. In order to take the account of physical reality, there has been a proclivity to move away from considering idealized mathematical problems in which the bounding wall is considered to be infinitesimally thin. Thus the conduction in solid wall and the convection in the fluid should be determined simultaneously. This type of convective heat transfer is referred to as a conjugate heat transfer (CHT) process and it arises due to the finite thickness of the wall. These types of problems have many practical applications, particularly those related to energy conservation in buildings, cold storage installations and cryogenic applications, such as medical and space technology and are studied extensively [3–5].

Also, with the growing importance of non-Newtonian fluids in modern technology and industries, the investigations on such fluids are desirable. Stokes [6] generalized the classical Newtonian model to include the effect of couple stresses in a way different from that of Eringen [7]. This is one among the several non-Newtonian fluid theories that are developed in the twentieth century. In his theory Stokes considered a body enclosing a volume without considering the microstructures of the infinitesimal fluid volume element. The set of all forces acting on an infinitesimal volume element is, in general, assumed to be equivalent to a single resultant force together with a resultant couple. The moment of the couple is assumed to be of non-zero value. With this assumption Stokes has proposed the theory of couple stress fluids allowing for the sustenance of couple stresses in addition to the usual stresses. Also, in his theory, curvature twist rate tensor is proposed based on the pure kinematic aspects of rotation vector and couple stress is defined in terms of this curvature twist rate tensor. Accordingly, in the balance of linear momentum of the couple stress flow model, fourth order derivatives of velocities are involved and, hence, separate angular momentum equation need not be considered. These fluids can also sustain the existence of body forces as usual and in addition to the body couples as well. The stress tensor is no longer symmetric in this theory. The fluids consisting of rigid, randomly oriented particles suspended in a viscous medium, such as blood, lubricants containing small amount of polymer additive, electro-rheological fluids and synthetic fluids are some of the examples for these couple stress fluids. This couple stress model has been widely used because of its great mathematical simplicity compared to that of the other models developed for the polar fluids. Recently, the study of couple stress fluid flows has been the subject of great interest, due to its widespread industrial and scientific applications as in the case of micropolar fluids. Important field where couple stress fluids have applications includes squeezing and lubrication [8],

☆ Communicated by A.R. Balakrishnan and T. Basak.

* Corresponding author.
E-mail address: hprani@nitw.ac.in (H.P. Rani).

0735-1933/$ – see front matter © 2013 Elsevier Ltd. All rights reserved.
http://dx.doi.org/10.1016/j.icheatmasstransfer.2013.08.015

Nomenclature

$\overline{C_f}$	dimensionless average skin-friction coefficient
c_p	specific heat at constant pressure
d_{ij}	rate of deformation tensor
g	acceleration due to gravity
Gr	Grashof number
k_f, k_s	thermal conductivity of the fluid and the solid cylinder, respectively
l	length of the cylinder
m	trace of couple stress tensor
m_{ij}	couple stress tensor
$\overline{Nu}$	average Nusselt number
P	conjugate-conduction parameter
p	fluid pressure
Pr	Prandtl number
r	radial coordinate
r_i, r_0	inner and outer radii of the hollow cylinder, respectively
R	dimensionless radial coordinate
t'	time
t	dimensionless time
t_{ij}	force stress tensor
T_0	temperature at the inside surface of the cylinder
T'	temperature of the fluid
u, v	velocity components in x, r directions, respectively
U, V	dimensionless velocity components in X, R directions, respectively
$\mathbf{U}$	velocity vector
x	axial coordinate
X	dimensionless axial coordinate

Greek Letters

α	thermal diffusivity
β	volumetric coefficient of thermal expansion
δ_{ij}	Kronecker delta
ε_{ijk}	Levi-Civita symbol
η, η'	couple stress viscosity coefficients
μ, λ	viscosity coefficients
$\omega_{i,j}$	spin tensor
$\boldsymbol{\omega}$	spin vector
Π'	heat function
Π	dimensionless heat function
ψ	dimensionless stream function
ρ	density
θ	dimensionless temperature of the fluid
ν	kinematic viscosity

Subscripts

w	conditions on the wall
∞	free stream conditions

bio-fluid mechanics [9], MHD flows and synthesis and plasticity of chemical compounds.

From the literature survey, it can be noted that the CHT on the unsteady natural convective flow of a viscous incompressible couple stress fluid past a vertical cylinder has received very scant attention in the literature. Hence, in the present investigation our attention is focused on the CHT problem of transient free convection over the outside surface of a vertical slender hollow cylinder. In general, studies on natural convection have been carried out with streamlines and isotherms. Note that, isotherms are generally used to illustrate the temperature distribution in a domain respectively, however, isotherms may not be suitable to visualize the direction and intensity of heat transfer particularly in convection problems in which the path of heat flux is not perpendicular to isotherms due to convection effect. When dealing with two-dimensional fluid flows, it is not the isobars but the streamlines that are the best tools for visualization and analysis, as fluid flows are not in the direction perpendicular to the isobars [10]. Similarly, when dealing with the two-dimensional convective heat transfer, it is not the isotherms but the heatlines that are the best tools for visualization and analysis. The main use of heatlines is to find the flow intensity in the region which is not observed in the other contours such as velocity and temperature. The heatlines are the more adequate tools for visualization and analysis of heat transfer process, giving well defined corridors where energy transfer occurs from the hot wall to the cold wall. The heatlines are mathematically represented by heat functions and the proper dimensionless forms of heat functions are closely related to the overall Nusselt numbers. The heatline concept was first introduced by Kimura and Bejan [11] and Bejan [12]. A detailed review on applications of heatlines and masslines was also performed by Costa [10]. The use of heatlines in the unsteady problems was first studied by Aggarwal and Manhapra [13,14] to analyze the unsteady heat transfer process in cylindrical enclosures subjected to natural convection. Recently, Basak et al. [15] studied the analysis of heatlines within triangular cavities. Till date, the heatline concept has been paid less attention for analyzing convective heat transfer processes except for very few applications. Based on this literature survey, an attempt is made for the first time to study the concept of heatlines for the present investigated problem.

In Section 2, description of the problem is given and the corresponding governing equations are derived. The details about the numerical method and the grid generation are explained. The average skin-friction and average heat transfer rate are also derived. In addition, heat function has been derived and non-dimensionalized based on the overall average Nusselt number on the hot wall. In Section 3, the comparison between the couple stress fluid flow and Newtonian fluid flow is analyzed. The average values of skin-friction and heat transfer rate with respect to time are shown graphically and discussed. Also the visualization of streamlines, isotherms and heatlines is shown. Finally, the concluding remarks are made in Section 4.

2. Mathematical formulation and simulation

A natural convective couple stress fluid flow past a vertical slender hollow cylinder of length l and the outer radius r_0 ($l >> r_0$) is considered as shown in Fig. 1. The x-axis is measured vertically upward along the axis of the cylinder. The origin of x is taken to be at the leading edge of the cylinder, where the boundary layer thickness is zero. The radial coordinate, r, is measured perpendicular to the axis of the cylinder. It is assumed that the fluid has constant physical properties and the fluid flow is unsteady, laminar and two-dimensional. The surrounding stationary fluid temperature is assumed to be of ambient temperature $\left(T'_\infty\right)$. The temperature of the inside surface of the cylinder is maintained at a constant temperature of T'_0, where $T'_0 > T'_\infty$. Initially, i.e., at time $t' = 0$ it is assumed that the outer surface of the cylinder and the fluid are of the same temperature T'_∞. As time increases ($t' > 0$), the temperature of the outer surface of the cylinder is raised to the solid-fluid interface temperature T'_w and maintained at the same level for all time $t' > 0$. It is assumed that the effect of viscous dissipation is negligible in the energy equation.

2.1. Governing equations

Based on the above assumptions and Boussinesq's approximation, the flow of an incompressible couple stress fluid in the absence of

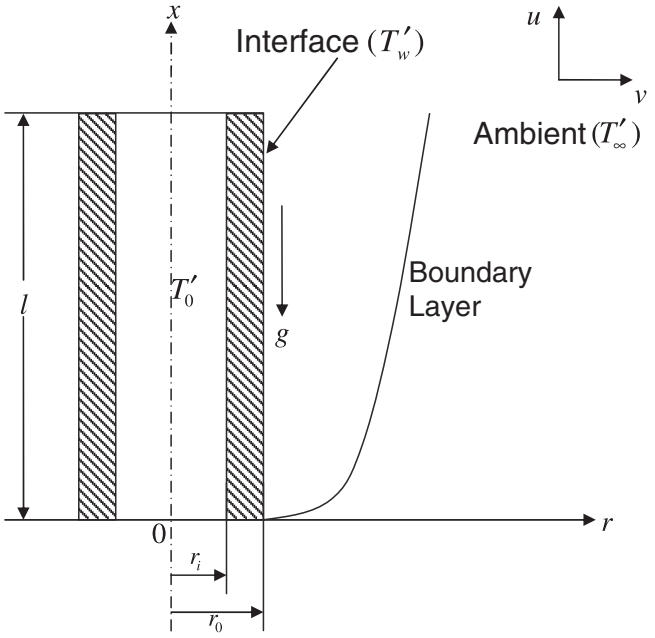

Fig. 1. Schematic of the investigated problem.

body force and body couple, the boundary layer equations along with the energy equation are as follows:

$$\frac{\partial(ru)}{\partial x}+\frac{\partial(rv)}{\partial r}=0 \tag{1}$$

$$\rho\left(\frac{\partial u}{\partial t'}+u\frac{\partial u}{\partial x}+v\frac{\partial u}{\partial r}\right)=\rho g\beta\left(T'-T_\infty'\right)+\frac{\mu}{r}\frac{\partial}{\partial r}\left(r\frac{\partial u}{\partial r}\right)-\eta\nabla^4 u \tag{2}$$

$$\frac{\partial T'}{\partial t'}+u\frac{\partial T'}{\partial x}+v\frac{\partial T'}{\partial r}=\frac{\alpha}{r}\frac{\partial}{\partial r}\left(r\frac{\partial T'}{\partial r}\right). \tag{3}$$

The constitutive equations concerning the force stress tensor t_{ij} and the couple stress tensor m_{ij} that arise in the theory of couple stress fluids are given by [6]

$$t_{ij}=(-p+\lambda\nabla.\mathbf{U})\delta_{ij}+2\mu d_{ij}-\frac{1}{2}\varepsilon_{ijk}\left[m_{,k}+4\eta\omega_{k,rr}+\rho c_k\right] \tag{4}$$

$$m_{ij}=\frac{1}{3}m\delta_{ij}+4\eta'\omega_{j,i}+4\eta\omega_{i,j}. \tag{5}$$

In the above Eqs. (4)–(5), $\mathbf{U}$ is the velocity vector, $\omega\left(=\frac{1}{2}\nabla\times\mathbf{U}\right)$ is the spin vector, $\omega_{i,j}$ is the spin tensor, d_{ij} is the rate of deformation tensor, $m(=m_{11}+m_{22}+m_{33})$ is the trace of the couple stress tensor m_{ij}, p is the fluid pressure, δ_{ij} is the Kronecker delta, ε_{ijk} is the Levi-Civita symbol and ρc_k is the body couple vector. Comma in the suffixes denotes covariant differentiation and $\omega_{k,rr}$ stands for $\omega_{k,11}+\omega_{k,22}+\omega_{k,33}$.

The quantities λ and μ are the viscosity coefficients and η, η' are the couple stress viscosity coefficients. These material constants are constrained by the following inequalities as,

$$\mu\geq 0;\ 3\lambda+2\mu\geq 0;\ \eta\geq 0;\ |\eta'|\leq\eta. \tag{6}$$

Usually, the ratio of material constants η and μ has the dimensions of length square i.e. $r_0^2\left(=\frac{\eta}{\mu}\right)$ (see Stokes [16]).

The initial and boundary conditions are given by:

$$\begin{array}{ll} t'=0: u=0,\ v=0,\ T'=T'_\infty & \text{for all } x \text{ and } r\\ t'>0: u=0,\ v=0,\ T'=T'_w & \text{at } r=r_0\\ u=0,\ v=0,\ T'=T'_\infty & \text{at } x=0\\ u\to 0,\ v\to 0,\ T'\to T'_\infty & \text{as } r\to\infty \end{array} \tag{7}$$

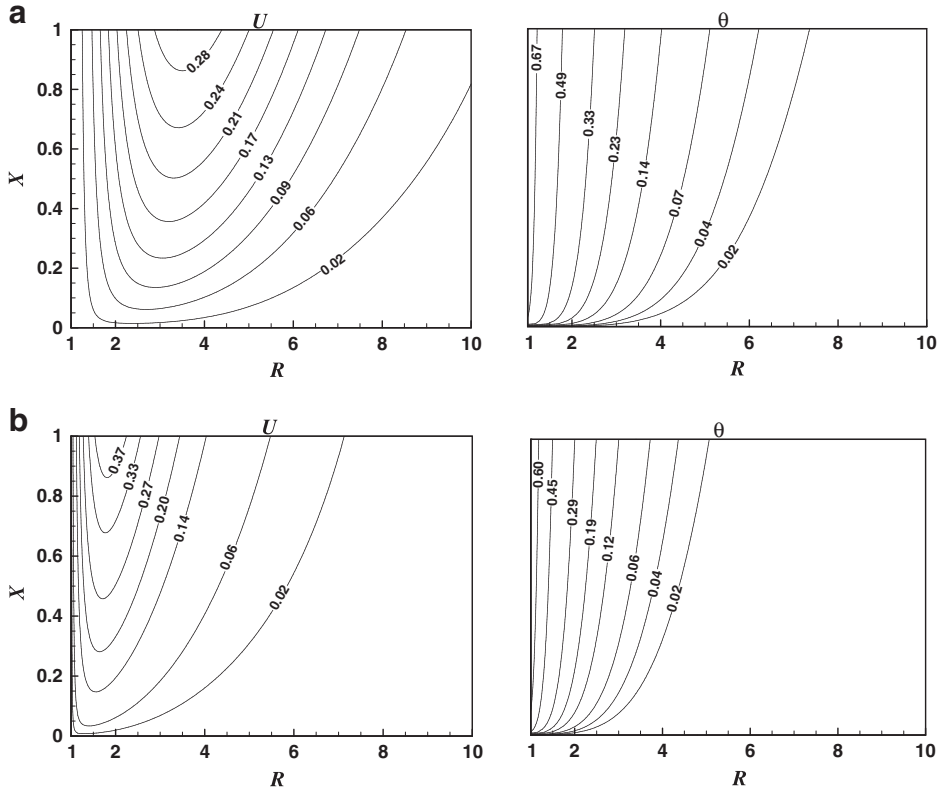

Fig. 2. Steady-state velocity (U) and temperature (θ) contours with $Pr=0.71$ and $P=0.5$ for (a) couple stress fluid; (b) Newtonian fluid.

where $T_w^{'}$ is the unknown solid-fluid interface temperature and is given by (Chang [17])

$$T_w^{'} = T^{'}(x, r_0) = r_0 \frac{k_f}{k_s} \ln\left(\frac{r_0}{r_i}\right) \frac{\partial T^{'}(x, r_0)}{\partial r} + T_0^{'} \quad \text{at} \quad r = r_0. \tag{8}$$

It can be noted that for couple stress fluids, the vorticity of the fluid on the boundary is equal to the rotational velocity of the boundary [16] i.e., Curl $\mathbf{U} = 0 \Rightarrow \frac{\partial u}{\partial r} = \frac{\partial v}{\partial x}$ at $r = r_0$ and as $r \to \infty$.

By introducing the following non-dimensional quantities

$$X = Gr^{-1}\frac{x}{r_0}, \quad R = \frac{r}{r_0}, \quad U = Gr^{-1}\frac{ur_0}{\nu}, \quad V = \frac{vr_0}{\nu}, \quad t = \frac{\nu t^{'}}{r_0^2}, \quad \theta = \frac{T^{'} - T_\infty^{'}}{T_0^{'} - T_\infty^{'}},$$
$$Gr = \frac{g\beta r_0^3\left(T_0^{'} - T_\infty^{'}\right)}{\nu^2}, \quad Pr = \frac{\nu}{\alpha}, \quad \alpha = \frac{k_f}{\rho c_p}, \quad P = \frac{k_f}{k_s}\ln\left(\frac{r_0}{r_i}\right) \tag{9}$$

(the symbols are explained in the nomenclature) in Eqs. (1)–(3), they were reduced to the following form:

$$\frac{\partial U}{\partial X} + \frac{\partial V}{\partial R} + \frac{V}{R} = 0 \tag{10}$$

$$\frac{\partial U}{\partial t} + U\frac{\partial U}{\partial X} + V\frac{\partial U}{\partial R} = \theta + \frac{\partial U}{\partial R}\left(\frac{1}{R} - \frac{1}{R^3}\right) + \frac{\partial^2 U}{\partial R^2}\left(1 + \frac{1}{R^2}\right) - \frac{2}{R}\frac{\partial^3 U}{\partial R^3} - \frac{\partial^4 U}{\partial R^4} \tag{11}$$

$$\frac{\partial \theta}{\partial t} + U\frac{\partial \theta}{\partial X} + V\frac{\partial \theta}{\partial R} = \frac{1}{Pr}\left(\frac{\partial^2 \theta}{\partial R^2} + \frac{1}{R}\frac{\partial \theta}{\partial R}\right). \tag{12}$$

The corresponding initial and boundary conditions are given by

$$\begin{aligned} &t = 0 : U = 0,\ V = 0,\ \theta = 0 && \text{for all } X \text{ and } R \\ &t > 0 : U = 0,\ V = 0,\ \theta - 1 = P\frac{\partial \theta}{\partial R} && \text{at } R = 1 \\ &\quad U = 0,\ V = 0,\ \theta = 0 && \text{at } X = 0 \\ &\quad U \to 0,\ V \to 0,\ \theta \to 0 && \text{as } R \to \infty \end{aligned} \tag{13}$$

$$\frac{\partial U}{\partial R} = \frac{1}{Gr^2}\frac{\partial V}{\partial X} \quad \text{at } R = 1 \text{ and as } R \to \infty.$$

In order to solve the unsteady coupled non-linear governing Eqs. (10)–(12) an implicit finite difference scheme of Crank–Nicolson type has been employed. The region of integration is considered as a rectangle composed of the lines indicating $X_{min} = 0$, $X_{max} = 1$, $R_{min} = 1$ and $R_{max} = 20 = 20$, where R_{max} corresponds to $R = \infty$ which lies very far from the momentum and energy boundary layers. The steady-state velocity and temperature values obtained with the grid system of 100×500 differ in the second decimal place from those with the grid system of 50×250, and differ in the fifth decimal place from those with the grid system of 200×1000. Hence, the grid system of 100×500 has been selected for all subsequent analyses, with the mesh sizes in X and R directions taken as 0.01 and 0.04, respectively. Also, the time step size dependency has been tested from which the step size 0.01 yielded a reliable result. The steady-state solution is assumed to have been reached when the absolute difference between the values of velocity as well as temperature at two consecutive time steps is less than 10^{-6} at all grid points.

2.2. Average skin-friction coefficient and heat transfer rate

Knowing the unsteady behavior of velocity and temperature profiles from the solution of Eqs. (10)–(12) along with the initial and boundary conditions in Eq. (13), it is worth to study the average skin-friction coefficient and the average heat transfer rate (Nusselt number). Increased skin-friction is generally a disadvantage in technical applications, while the increased heat transfer can be exploited in some applications such as heat exchangers, but should be avoided in others such as gas turbine applications, for instance. The non-dimensional average skin-friction coefficient and Nusselt number are given by $\overline{C_f} = \int_0^1 \left(\frac{\partial U}{\partial R}\right)_{R=1} dX$ and $\overline{Nu} = -\int_0^1 \left(\frac{\partial \theta}{\partial R}\right)_{R=1} dX$, respectively. The derivatives are evaluated by using a five-point approximation formula and then the integrals are evaluated by using the Newton–Cotes closed integration formula.

2.3. Stream and heat functions

The relationships between the stream function, ψ and velocity components for two-dimensional flows are $U = \frac{1}{R}\frac{\partial \psi}{\partial R}$ and $V = -\frac{1}{R}\frac{\partial \psi}{\partial X}$.

The heat function Π' is defined through its first-order derivatives as

$$\frac{\partial \Pi^{'}}{\partial x} = \rho r v c_p\left(T^{'} - T_\infty^{'}\right) - k_f r\frac{\partial T^{'}}{\partial r} \tag{14a}$$

$$-\frac{1}{r}\frac{\partial \Pi^{'}}{\partial r} = \rho u c_p\left(T^{'} - T_\infty^{'}\right). \tag{14b}$$

Introducing the non-dimensional heat function $\Pi = \frac{\Pi^{'}}{k_f\left(T_0^{'} - T_\infty^{'}\right) r_0 Gr}$, to make the heat function as dimensionless so that its maximum value

Table 1
Comparison between the (i) couple stress fluid and (ii) Newtonian fluid flows for different values of Pr and P in terms of the (a) flow variables (U, θ) and (b) average values of C_f and Nu.

Pr	P	Temporal maximum (t) of		Steady-state time (t)	Maximum velocity (U) at $X = 1.0$
		U	θ		
a(i)					
0.71	0.5	8.05	8.09	14.03	0.3043
1.0	0.5	8.96	9.10	14.81	0.2678
2.0	0.5	11.42	11.86	15.18	0.2038
3.0	0.5	13.35	14.09	16.79	0.1722
0.71	0.1	7.00	6.97	13.31	0.3382
0.71	1.0	9.11	9.21	14.74	0.2749
0.71	2.0	10.81	10.96	15.79	0.2371
a(ii)					
0.71	0.5	6.01	5.77	14.87	0.4013
1.0	0.5	6.27	6.04	14.53	0.3785
2.0	0.5	7.04	6.85	14.00	0.3242
3.0	0.5	7.68	7.52	13.93	0.2896
0.71	0.1	4.94	4.68	13.97	0.4706
0.71	1.0	7.05	6.81	15.66	0.3491
0.71	2.0	8.68	8.39	16.78	0.2892

Pr	P	$\overline{C_f}$	$\overline{Nu}$
b(i)			
0.71	0.5	0.1606	0.6988
1.0	0.5	0.1461	0.7359
2.0	0.5	0.1194	0.8140
3.0	0.5	0.1054	0.8621
0.71	0.1	0.1882	0.7131
0.71	1.0	0.1380	0.6843
0.71	2.0	0.1109	0.6627
b(ii)			
0.71	0.5	1.0481	1.0491
1.0	0.5	1.0031	1.0931
2.0	0.5	0.8932	1.2107
3.0	0.5	0.8209	1.2979
0.71	0.1	1.3106	1.0876
0.71	1.0	0.8657	1.0111
0.71	2.0	0.6714	0.9585

equals the overall Nusselt number on the hot wall (see Refs. [11,13]) and Eqs. (14a) and (14b) rewritten as

$$\frac{\partial \Pi}{\partial X} = Pr(RV\theta) - R\frac{\partial \theta}{\partial R} \tag{15a}$$

$$-\frac{\partial \Pi}{\partial R} = Pr(RU\theta). \tag{15b}$$

Note that the functions Π' and Π, identically satisfy the steady-state form of the dimensional and non-dimensional energy equations (Eqs. (3) and (12)), respectively. The boundary conditions of Π are taken from Eqs. (15a) and (15b). Further details can be found elsewhere [11,13].

3. Results and discussion

The steady-state velocity (U) and temperature (θ) profiles in the case of Newtonian fluids are compared with the existing results of Lee et al. [2] and found to be in good agreement. Fig. 2 illustrates the steady-state U and θ contours for couple stress and Newtonian fluid flows with fixed $Pr = 0.71$ and $P = 0.5$. It can be noticed that from Fig. 2a and b, the velocity of the couple stress fluid flow is much less compared to that of the Newtonian fluid flow, while the opposite trend is observed for the temperature. This is due to the fact that in couple stress fluid flow there are additive diffusion terms (biharmonic term) compared with that of the Newtonian fluid flow (refer Eq. (11)). Also, from Fig. 2a and b it is observed that the steady-state temperature contours for the couple stress fluid are somewhat different, with thicker temperature layer, from those of the Newtonian fluid.

Table 1 explains the variation between the couple stress fluid and Newtonian fluid flows in terms of the flow variables to reach the temporal maximum and the steady-state with different Pr and P values. Also, it explains the variation with respect to $\overline{C_f}$ and $\overline{Nu}$. Table 1a(i) and a(ii) tabulates values for the times to reach the temporal maxima and steady-state, respectively. It is observed that for all values of Pr and P the times needed for all the flow variables to reach the temporal maxima for the couple stress fluid flow are larger than those of the Newtonian fluid flow. It is also noticed that with the increasing values of P, the times required for all the flow variables to reach the steady-state for the couple stress fluid flow are rather smaller than those for the Newtonian fluid flow. This implies that the transient periods, after the temporal maxima, are quite longer for the Newtonian fluid flow compared to those for the couple stress fluid flow. While the opposite trend is observed for Pr. Also, for all values of Pr and P, the velocity of a couple stress fluid flow is decreased in comparison with that of the Newtonian fluid flow. From Table 1b(i) and b(ii), it is noticed that the average values of skin-friction coefficient decrease as Prandtl number (Pr) and conjugate-conduction parameter (P) increase. On the other hand it can be observed that an increase in the P is associated with a decrease in the local rate of heat transfer i.e., for poor conductive wall, the average Nusselt number has low values. This is a logical result since reducing the thermal conductivity of the wall leads to the increase in thermal resistance of the overall system and therefore reducing the Nusselt number. Natural convection in the fluid part is very slow and conduction heat transfer dominates in this case as shown in Fig. 3b (i) and(ii). Also, thus, from Table 1b(i) and b(ii), it is observed that the $\overline{C_f}$ and $\overline{Nu}$ of a couple stress fluid flow are smaller than that of the Newtonian fluid flow for all values of Pr and P. In summary, Table 1b reveals that the wall shear stress and heat transfer rate of a couple stress fluid flow differ from those of the Newtonian fluid flow.

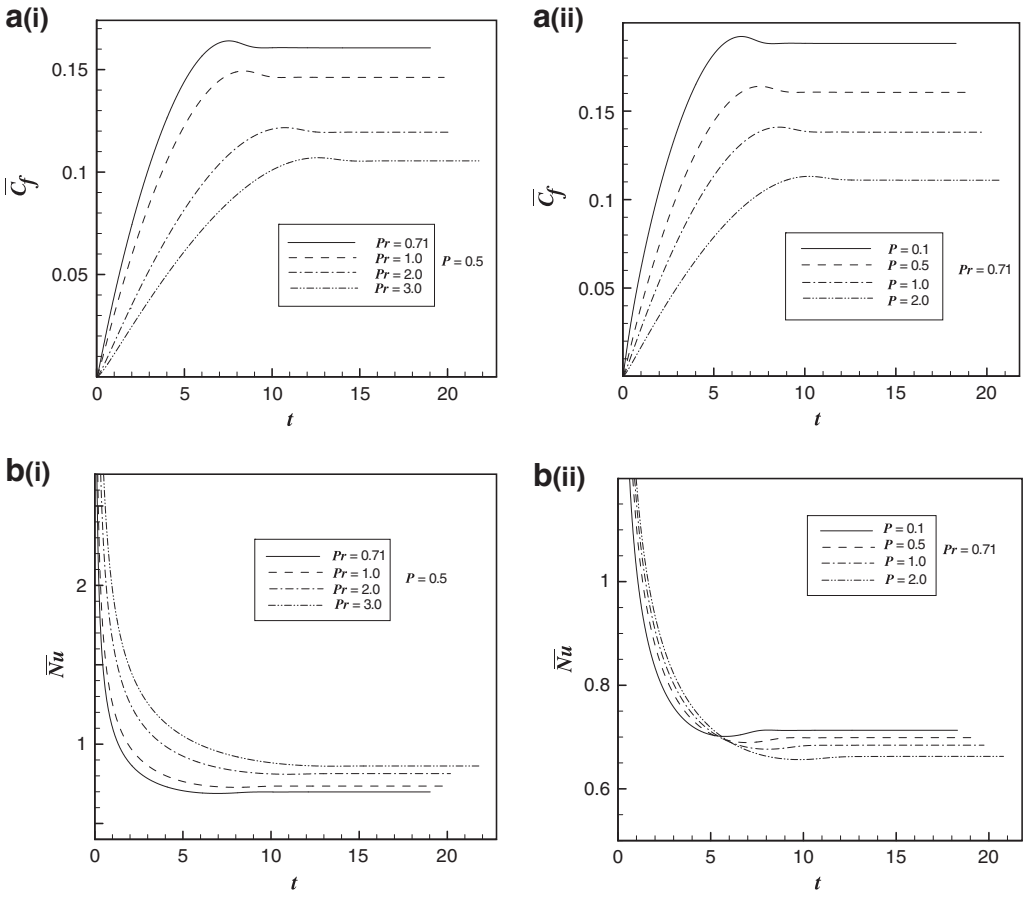

Fig. 3. The simulated average (a) skin-friction $\left(\overline{C_f}\right)$ and (b) Nusselt number $(\overline{Nu})$ for variation of (i) Pr and (ii) P.

The effects of *Pr* and *P* on the simulated $\overline{C_f}$ and $\overline{Nu}$ are shown graphically in Fig. 3a and b, respectively. From Fig. 3a(i) and a(ii) it is observed that for all values of *Pr* and *P* the $\overline{C_f}$ increases at first with time, attains the peak values and, after slight decreasing, reaches the steady-state asymptotically. For increasing values of *Pr* the values of $\overline{C_f}$ decrease. Similar trend is observed for *P*. It is related to the fact that the increased value of *P* decreases the velocity of the fluid within the boundary layer and decreases the viscosity of the fluid. During the initial period, the variation of $\overline{C_f}$ with respect to *P* is larger than *Pr*. This implies that the $\overline{C_f}$ is more strongly affected by *P* in comparison to *Pr*. From Fig. 3b(i) and b(ii) it is observed that after $t = 0$, for short period of time, the $\overline{Nu}$ is almost the same for all values of *Pr* and *P*. This shows that initially heat conduction is dominating in comparison with the convection. Fig. 3b(i) reveals that an increase in the value of *Pr* leads to an increase in the values of the $\overline{Nu}$. Increasing *Pr* speeds up the spatial decay of the temperature near the heated surface together with increased flow velocity near the wall, yielding an increase in the rate of heat transfer. With the increasing values of *P* i.e. with lower wall conductance (k_s), initially, $t \leq 5.57$, the $\overline{Nu}$ is almost the same with an increasing trend. Later it decreases with increasing values of *P* and attains the steady-state.

Fig. 4 illustrates the streamlines, isotherms and heatlines at the steady-state for different values of *Pr* and *P*. It is observed that the variation in heatlines and isotherms occurs very close to the hot wall in comparison to that of streamlines. The streamlines are denser near the

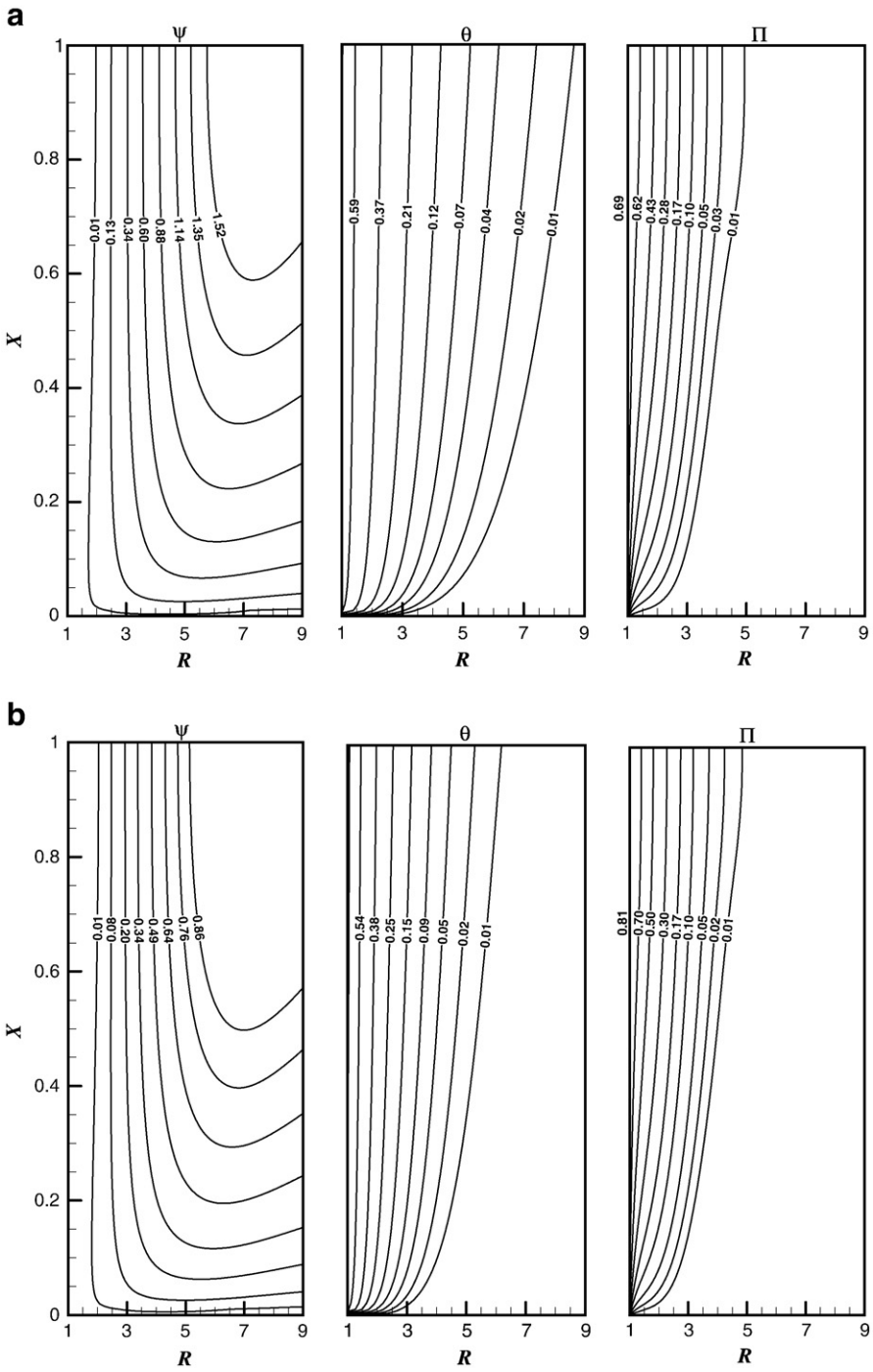

Fig. 4. Simulated steady-state stream function (ψ), temperature (θ) and heat function (Π) contours for (a) $Pr = 0.71$, $P = 0.5$; (b) $Pr = 2.0$, $P = 0.5$; and (c) $Pr = 2.0$, $P = 2.0$.

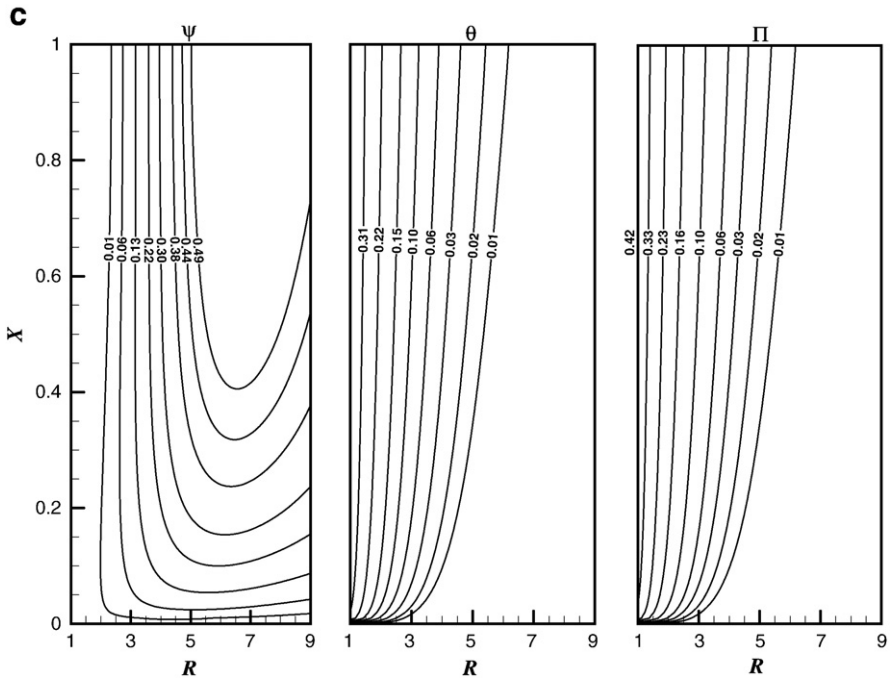

Fig. 4 (*continued*).

leading edge of the cylinder. The intensity of the heat transfer from the hot wall to the fluid is maximum for increasing values of X, and it decreases as X decreases. The heatlines near the wall being straighter for higher X values. It is also noticed that the relevant heat transfer phenomena occur inside the thermal boundary layer, as assumed by the boundary layer hypothesis. From Fig. 4a and b it is observed that as Pr increases, the maximum value of Π increases since $\overline{Nu}$ increases on the hot wall as shown in Table 1b(i). Also the deviation of heatlines from the hot wall is more, while the reverse trend is observed for the case of isotherms. Fig. 4b and c shows that as P increases, the maximum value of Π decreases since $\overline{Nu}$ decreases with P. It is noticed that the heatlines tend to move away from the hot wall for higher values of P, but there is no such variation in the case of isotherms. This is due to the reason that the isotherms are identified by the temperature levels in the domain, but they are poor and inadequate tools for heat transfer visualization and analysis.

4. Conclusions

Extensive heat flow visualization is employed to study the conjugate heat transfer effects for an unsteady natural convective couple stress fluid flow over a vertical slender hollow cylinder. The non-dimensional governing equations are derived and solved numerically. When properly made dimensionless, the numerical values of the heat function are closely related to the overall Nusselt number, which characterize the overall heat transfer process. The flow visualization includes the plots of streamlines, isotherms and heatlines. The basic characteristics of heat lines are useful for perceiving the visualization results and also it has been shown that the level of heatlines is a direct measure of the heat transfer. The computations are carried out for different values of Pr and conjugate-conduction parameter P. It is observed that the average skin-friction coefficient decreases with the increasing values of Pr and P. It is also noticed that the steady-state values of average heat transfer rate decrease with increasing P and decreasing Pr. Boundary layer flow visualization indicates that the heatlines occur in the vicinity of the hot wall. Also, it is observed that as Pr and P increase, the deviations of heatlines from the hot wall increase. Particularly, this study reveals that the deviations of velocity and temperature profiles of couple stress fluid flow from those of the Newtonian fluid flow turn out to be considerable.

Acknowledgments

The authors are thankful to the reviewers for their valuable suggestions and comments to improve the quality of the manuscript.

References

[1] T. Fujii, H. Uehara, Laminar natural convective heat transfer from the outer surface of a vertical cylinder, Int. J. Heat Mass Transf. 13 (3) (1970) 607–615.
[2] H.R. Lee, T.S. Chen, B.F. Armaly, Natural convection along slender vertical cylinders with variable surface temperature, J. Heat Transf. 110 (1) (1988) 103–108.
[3] M. Miyamoto, J. Sumikawa, T. Akiyoshi, T. Nakamura, Effects of axial heat conduction in a vertical flat plate on free convection heat transfer, Int. J. Heat Mass Transf. 23 (11) (1980) 1545–1553.
[4] I. Pop, B. Ingham, Y. Yuan, Mixed convective conjugate heat transfer from a vertical flat plate, ZAMM-Z. Angew. Math. Mech. 76 (5) (1996) 281–289.
[5] A. Kaya, Effects of buoyancy and conjugate heat transfer on non-Darcy mixed convection about a vertical slender hollow cylinder embedded in a porous medium with high porosity, Int. J. Heat Mass Transf. 54 (4) (2011) 818–825.
[6] V.K. Stokes, Couple stress in fluids, Phys. Fluids 9 (9) (1966) 1709–1715.
[7] A.C. Eringen, Theory of micropolar fluids, J. Math. Mech. 16 (1966) 1–18.
[8] C. Chang-Jian, H. Yau, J. Chen, Nonlinear dynamic analysis of a hybrid squeeze-film damper-mounted rigid rotor lubricated with couple stress fluid and active control, Appl. Math. Model. 34 (9) (2010) 2493–2507.
[9] V.P. Srivastava, Flow of a couple stress fluid representing blood through stenotic vessels with a peripheral layer, Indian J. Pure Appl. Math. 34 (12) (2003) 1727–1740.
[10] V.A.F. Costa, Bejan's heatlines and masslines for convection visualization and analysis, Appl. Mech. Rev. 59 (3) (2006) 126–145.
[11] S. Kimura, A. Bejan, The heatline visualization of convective heat transfer, J. Heat Transf. 105 (4) (1983) 916–919.
[12] A. Bejan, Convection Heat Transfer, third ed. Wiley, New York, 2004. 76–82.
[13] S.K. Aggarwal, A. Manhapra, Use of heatlines for unsteady buoyancy-driven flow in a cylindrical enclosure, J. Heat Transf. 111 (2) (1989) 576–578.
[14] S.K. Aggarwal, A. Manhapra, Transient natural convection in a cylindrical enclosure nonuniformly heated at the top wall, Numer. Heat Transfer, Part A 15 (3) (1989) 341–356.
[15] T. Basak, G. Aravind, S. Roy, A.R. Balakrishnan, Heatline analysis of heat recovery and thermal transport in materials confined within triangular cavities, Int. J. Heat Mass Transf. 53 (2010) 3615–3628.
[16] V.K. Stokes, Theories of Fluids with Microstructure, Springer-Verlag, New York, 1984. 34–80.
[17] C. Chang, Buoyancy and wall conduction effects on forced convection of micropolar fluid flow along a vertical slender hollow circular cylinder, Int. J. Heat Mass Transf. 49 (2006) 4932–4942.